REGULAR ARTICLE

Feasibility of human hair follicle-derived mesenchymal stem cells/CultiSpher®-G constructs in regenerative medicine

Pengdong Li[1,3] · Feilin Liu[1] · Chunling Wu[4] · Wenyue Jiang[2] · Guifang Zhao[1] · Li Liu[1] ·
Tingting Bai[1] · Li Wang[1] · Yixu Jiang[1] · Lili Guo[5] · Xiaojuan Qi[1] · Junna Kou[1] ·
Ruirui Fan[1] · Deshun Hao[1] · Shaowei Lan[1] · Yulin Li[1] · Jin Yu Liu[1,3]

Abstract The use of human mesenchymal stem cells (hMSCs) in cell therapies has increased the demand for strategies that allow efficient cell scale-up. Preliminary data on the three-dimensional (3D) spinner culture describing the potential use of microcarriers for hMSCs culture scale-up have been reported. We exploited a rich source of autologous stem cells (human hair follicle) and demonstrated the robust in vitro long-term expansion of human hair follicle-derived mesenchymal stem cells (hHF-MSCs) by using CultiSpher®-G microcarriers. We analyzed the feasibility of 3D culture by using hHF-MSCs/CultiSpher®-G microcarrier constructs for its potential applicability in regenerative medicine by comparatively analyzing the performance of hHF-MSCs adhered to the CultiSpher®-G microspheres in 3D spinner culture and those grown on the gelatin-coated plastic dishes (2D culture), using various assays. We showed that the hHF-MSCs seeded at various densities quickly adhered to and proliferated well on the microspheres, thus generating at least hundreds of millions of hHF-MSCs on 1 g of CultiSpher®-G within 12 days. This resulted in a cumulative cell expansion of greater than 26-fold. Notably, the maximum and average proliferation rates in 3D culture were significantly greater than that of the 2D culture. However, the hHF-MSCs from both the cultures retained surface marker and nestin expression, proliferation capacity and differentiation potentials toward adipocytes, osteoblasts and smooth muscle cells and showed no significant differences as evidenced by Edu incorporation, cell cycle, colony formation, apoptosis, biochemical quantification and qPCR assays.

Pengdong Li and Feilin Liu contributed equally to this work.

✉ Jin Yu Liu
  jy_liu@jlu.edu.cn

[1] Department of Pathobiology, Key Laboratory of Ministry of Education, Norman Bethune College of Medicine, Jilin University, Changchun, Jilin 130021, People's Republic of China

[2] Department of Analytical Chemistry, School of Pharmaceutical Sciences, Jilin University, Changchun, Jilin 130021, People's Republic of China

[3] Department of Toxicology, School of Preventive Medicine, Jilin University, Changchun, Jilin 130021, People's Republic of China

[4] Harbin Veterinary Research Institute, CAAS-Michigan State University Joint Laboratory of Innate Immunity, State Key Laboratory of Veterinary Biotechnology, Chinese Academy of Agricultural Sciences, Maduan Street 427, Nangang District, Harbin 150001, People's Republic of China

[5] Department of Pathology, Jilin Cancer Hospital, Changchun, Jilin 130012, People's Republic of China

Introduction

Cell therapy is emerging as a promising strategy for tissue repair and regeneration. This approach is hampered, however, by the lack of large amounts of human autologous stem cell sources with higher proliferative and multipotent differentiation potential (Chen et al. 2013; Lutz et al. 2014; Motaln et al. 2010; Pittenger et al. 1999). Although large-scale expansion of stem cells is possible by repeated sub-culturing, their efficacy for use in the regenerative medicine is compromised due to replicative cell senescence and loss of multipotency associated with repeated subcultures. Mesenchymal stem cells (MSCs) dosage per treatment for stem cell therapies can range

between 50,000 and 6 billion cells. The applicability of the current 2-dimensional tissue culture platform is limited to low cell doses and becomes less feasible in presence of doses above 50 million (Chen et al. 2013). Such high doses would make the current 2D cell culture platform technically and economically untenable, especially under clinical settings. This necessitates the use of 3D culture for high-density expansion and efficient differentiation of human stem cells in vitro. Several studies have demonstrated the potential beneficial effects of 3D cultivation strategies (Chen et al. 2011; Choi et al. 2011; Sart et al. 2009; Yang et al. 2007).

In recent years, research has demonstrated the feasibility of a microcarrier–stem cell culture approach, especially by using microbeads in 3D scaffolds (Chen et al. 2013; Martin et al. 2011; Sun et al. 2010). Microbeads have a large surface-to-volume ratio, thus offering large accessible surfaces for cell growth in small culture volumes in vitro and thereby enabling the robust expansion of anchorage-dependent cells (Chen et al. 2013; Sart et al. 2013; Sun et al. 2011), such as MSCs, without the need for repeated sub-culturing for subsequent stem cell therapy. In addition to serving as biocompatible-biodegradable carriers for culturing cells, microbeads could be used as cell-delivery vehicles to directly deliver the cultured cells into an implanted scaffold (Liu et al. 2004b). This direct transplantation of cell-laden vehicles precludes the essential step of releasing the stem cells from culture carriers such as, tissue culture plates, flasks, or from non-biodegradable microbeads by trypsinization, which has been proved to be detrimental to cell-adhesion molecules, wherein it results in cell senescence and loss of multipotency. Several recent studies have demonstrated the large-scale generation of human MSCs from bone marrow (Yang et al. 2007), adipose tissue (Choi et al. 2011), placenta (Chen et al. 2011; Timmins et al. 2012) and ear (Sart et al. 2009) by using microbeads as microcarriers for 3D culture. It is therefore imperative to consider microbead-based microcarriers as the alternative platform.

Among the various microcarrier cultures, the macroporous microcarriers, namely Cytopore and CultiSpher, offer higher cell surface areas for growth and a better mechanical protection to the cells from shear stress generated by stirrers, spargers or spin filters (Chen et al. 2013; Martin et al. 2011). Interestingly, previous studies that screened various microcarrier cultures for the propagation of MSCs demonstrated CultiSpher S to yield the highest cell attachment rate (over 90 % efficiency) and a 15-fold cell expansion with a seeding efficiency of over 70 % in a spinner flask system (Timmins et al. 2012).

Apart from microcarrier culture, 3D culture of cell aggregates has been developed to reduce the cost and simplify cell harvesting. Although the aggregate culture has demonstrated scalability and achieved up to 1.89×10^6 cells/mL (17.7-fold expansion), the formation of homogeneous aggregates with consistent size poses a challenge due to significant loss of initial cell viabilities (28–76 %) during aggregate formation (Olmer et al. 2010). Moreover, disaggregation, which is usually performed through manual manipulation, undermines the scalability of this platform.

Human air follicles (hHF) are easily accessible and harbor a rich autologous stem cell pool with mesenchymal lineage differentiation potential. Accumulating evidence has suggested that hHF-MSCs are true stem cells that possess multi-lineage (myogenic, osteogenic, adipogenic and chondrogenic lineages) differentiation potential (Amoh et al. 2005b; Jahoda et al. 2003; Liu et al. 2010). The study by Bajpai et al. demonstrated a higher proliferative capacity of hHF-MSCs in comparison with bone marrow (BM)-MSCs and further showed that hHF-MSCs upon differentiation express lineage-specific genes in chronological order and to a considerable extent (Bajpai et al. 2012). hHF-MSCs have been used as cell sources to engineer functional vascular grafts (Peng et al. 2011), to re-establish hematopoietic tissues (Lako et al. 2002), to reconstruct full-thickness skin (Shim and Han 2007) and to deliver release-controlled insulin gene (Wu et al. 2014) and promising results have been obtained from both clinical and preclinical settings. Very promisingly, stem cells from hair follicle express a protein marker for neural stem cells and transdifferentiate largely into Schwann cells, which are known to support neuron regrowth and be used as a cell source for efficient treatment of peripheral nerve injury (Amoh et al. 2005a, c, 2008; Duong et al. 2012; Hoffman 2007; Li et al. 2003; Liu et al. 2011; Mii et al. 2013; Uchugonova et al. 2011). In addition, the use of induced pluripotent stem cells derived from human hair follicles that are genetically identical to the donor, does not raise any ethical conflicts nor does it involve immune rejection problems in the event of autologous implantation (Higgins et al. 2012; Wang et al. 2013).

Many previous reports (Sart et al. 2013; Schop et al. 2010; Sun et al. 2010) have provided preliminary spinner culture data describing the potential use of bead-to-bead cell transfer for MSCs culture scale-up. However, a comparative analysis of the performance of hHF-MSCs adhered to the CultiSpher®-G microspheres in 3D spinner culture and those grown on the conventional 2D culture has not yet been clarified.

In view of the above and the need for large-scale generation of MSCs, in the present study, we exploited the readily accessible, rich source of autologous stem cells, the human hair follicles, in order to demonstrate the robust in vitro long-term expansion of hHF-MSCs by using CultiSpher®-G microcarriers. Further, we analyzed the feasibility of 3D culture using hHF-MSCs/CultiSpher®-G microcarrier constructs for their potential applicability in regenerative medicine, by comparing the proliferation and differentiation potentials of the hHF-MSCs grown in gelatin-coated 24-well plates and

in spinner bottles with hHF-MSCs adhered to the CultiSpher®-G microcarriers.

Materials and methods

The present study was approved by the Ethics Committee of the Norman Bethune College of Medicine, Jilin University. After informed written consent was obtained, hHF-MSCs were obtained by plucking the hair follicles from the occipital region of the scalp of three volunteers (27-year-old female, 29-year-old male and 49-year-old male).

Isolation and cultivation of hHF-MSCs

The isolation and cultivation of hHF-MSCs in 24-well plates were performed as described elsewhere (Liu et al. 2008; Wang et al. 2013; Zhang et al. 2013). Briefly, about 40–60 hairs were plucked from the occipital region of each of three volunteers. Those hairs with intact hair follicles were pooled and extensively washed in phosphate-buffered saline (PBS; Life Technologies, Carlsbad, CA, USA) containing 1 % penicillin/streptomycin solution (P/S, 100 IU/mL penicillin, 100 IU/mL streptomycin; Hyclone, Victoria, Australia). After washing, the hair shafts were cut off and the remaining portions of the hairs were manually placed on the bottom of a 24-well plate (Corning, NY, USA), one piece of hair per well and cultured in 200 μL of Dulbecco's modified Eagle medium:Nutrient Mixture F-12 (DMEM/F-12; Life Technologies) containing 10 % fetal bovine serum (FBS; Hyclone), 1 % P/S and 10 ng/mL basic fibroblast growth factor (bFGF; PeproTech, London, UK) at 5 % CO_2 and 37 °C overnight. The next day, 400 μL of culture medium was added into the well and the medium was changed every 3 days. Seven to ten days after the initiation of the hair follicle culture, the cells migrating out from the hair follicles were harvested and their morphological characteristics were examined under a microscope. The hair follicle cells exhibited either cobblestone, or spindle-shaped morphology. Those cells with the spindle shape were trypsinized (0.25 % EDTA-Trypsin; Life Technologies), pooled and expanded as described previously (Liu et al. 2010; Wang et al. 2013; Zhang et al. 2013).

Preparation of CultiSpher®-G microcarriers

CultiSpher®-G microcarriers beads (diameter 130–380 μm) were obtained from Sigma-Aldrich (St. Louis, MO, USA) and were prepared according to the manufacturer's instructions. They represent macroporous gelatin beads in which the hHF-MSCs have the ability to use the interior surface. Briefly, for their preparation, dry microcarriers (1 g dry CultiSpher®-G/30 mL) were swollen and hydrated in calcium

and magnesium-free PBS for 12 h at room temperature (RT). Without removing the PBS, the microcarriers were sterilized by autoclaving at 121 °C and 14.5 psi (about 1 bar) for 30 min. Consequently, the PBS was removed and the microcarriers were washed one time in culture medium.

Preparation of gelatin-coated culture dishes

Gelatin (Sigma-Aldrich) was dissolved in deionized water and sterilized by autoclaving at 121 °C and 14.5 psi (about 1 bar) for 30 min. Culture dishes were coated with 0.2 % gelatin solution for 4 h at 37 °C in 5 % CO_2; excess solution was removed without rinsing. After drying in a laminar flow hood, the coated culture dishes were used immediately for initiation of the 2D culture.

In vitro expansion of hHF-MSCs in CultiSpher®-G by 2D and 3D culture

The hHF-MSCs from passage 5 were seeded separately in both the spinner culture and the conventional 2D culture, to achieve final densities of 0.5×10^3, 1.0×10^3 or 2.0×10^3 cells/cm^2. For the production of adherently growing hHF-MSCs, macroporous CultiSpher®-G gelatin microcarriers were used in concentration of 1 g/100 mL (1 g of CultiSpher®-G has a total surface area of 1 m^2). The hHF-MSCs in the spinning bottles (CELLspin; Integra Biosciences, Chur, Switzerland) filled with 100 mL DMEM/F-12 supplemented with 10 % FBS and 10 ng/mL bFGF were incubated for 8 days at 37 °C in 5 % CO_2, over the magnetic stirrer at a stirring rate of 60 rpm, with intermittent stirring for 5 min after a gap of 30 min. The culture medium was changed every 3 days. The hHF-MSCs cultured on a gelatin-coated 24-well plate (2D culture) served as controls. The entrapment of the cells was observed before and after the stirring. Cell entrapment was monitored using a inverted fluorescence microscope (Leica DMI4000B; Leica Microsystems, Germany), equipped with a DCF 310 FX digital camera (Leica Microsystems).

Cell proliferation assay

Aliquots of hHF-MSCs-CultiSpher®-G microcarrier constructs were removed from the spinning bottles on days 2, 4, 6 , 8, 10 and 12, respectively. They were then transferred, in triplicate, into 2-mL Eppendorf tubes (1 mL per tube; Axygen, Union City, CA, USA) and kept still for 5 min to allow the hHF-MSCs-CultiSpher®-G microcarrier constructs to settle to the bottom of the Eppendorf tubes. After removing the culture medium by aspiration, the hHF-MSCs adhered to the CultiSpher®-G microspheres, as well as those in the gelatin-coated 24-well plate, were washed in PBS and then separately digested with 0.25 % EDTA-Trypsin (37 °C, 15 min, 5 min) to completely dissociate the microcarriers or release hHF-MSCs

from the gelatin-coated 24-well plate. The cells obtained from both procedures were counted using the hemocytometer cell counting chamber (Shanghai Qiujing, Shanghai, China), as described previously (Phillips and Terryberry 1957; Sun et al. 2010). Cell viability was determined by performing the trypan blue (0.4 % in normal saline; Life Technologies) dye exclusion test using the cell counter. The proliferation curves of hHF-MSCs from the 3D and 2D cultures were plotted with the number of cell/mL released from CultiSpher®-G or tissue culture plate indicated on the y-axis and the time period (in days) indicated on the x-axis.

The average cell proliferation rate (μ_{avg}) was calculated as follows: (maximum cell number − seeding cell number) / culture time (h). The maximum cell proliferation rate (μ_{max}) was calculated as follows: (maximum cell number at the exponential phase − minimal cell number at the exponential phase) / culture time (h) at the exponential phase (Sun et al. 2009, 2010).

Acridine orange staining

Acridine orange staining was performed on CultiSpher®-G microcarrier constructs from the 3D culture. Acridine orange is a cell-permeable, nucleic acid selective fluorescent cationic dye that interacts with DNA or RNA and forms the corresponding complexes, which when excited by an appropriate wavelength emit green or red fluorescence, respectively (Hayashi et al. 1983). To localize the growth of hHF-MSCs on the CultiSpher®-G microcarriers, aliquots of hHF-MSCs-CultiSpher®-G microcarrier constructs were removed from the spinning bottle on days 2, 4, 6 , 8, 10 and 12, respectively, washed with PBS and fixed in 4 % paraformaldehyde (10 min; Beijing Dingguo, Beijing, China) at RT. After the removal of paraformaldehyde by aspiration, the microcarrier constructs were washed with PBS, and were subsequently incubated with 0.1 mg/mL of acridine orange (37 °C, 15 min; Beijing Dingguo). At the end of the incubation period, the microcarrier constructs were washed again with PBS, transferred onto a 35-mm tissue culture plate (Corning) and were visualized using a inverted fluorescence microscope. The negative control comprised CultiSpher®-G microcarriers alone.

5-Ethynyl-2′-deoxyuridine incorporation and flow cytometry assay

In addition, cell proliferation assay with "click" chemistry was performed to detect the progression of S-phase in the hHF-MSCs by using 5-Ethynyl-2′-deoxyuridine (EdU), a thymidine analogue, which is incorporated into the DNA of dividing cells during the S-phase of the cell cycle. The incorporated EdU could be detected through a reaction between the alkyne group of EdU and the fluorescent azide in a copper-catalyzed azide-alkyne cycloaddition (Salic and Mitchison 2008).

Briefly, on day 6, the hHF-MSCs from the 2D culture and the CultiSpher®-G microcarrier constructs (200 μL) from the 3D culture were incubated in triplicate in a fresh medium containing 10 μM of EdU (Guangzhou Ruibo, Guangzhou, China) for 24 h at 37 °C in 5 % CO_2. At the end of the incubation period, the hHF-MSCs from both the cultures were fixed with 4 % paraformaldehyde for 10 min at RT. After discarding the fixative, the hHF-MSCs were incubated with 2 mg/mL of glycine for 5 min and then washed thrice in PBS. Subsequently, they were again incubated with 0.5 % TritonX-100 (Sigma-Aldrich) for 15 min at RT and finally stained with Apollo® 488 solution (Guangzhou Ruibo) for 30 min at RT, according to the manufacturer's instructions. After washing with PBS and methanol (Beijing Huagongchang, Beijing, China), the hHF-MSCs from both the cultures were counterstained with Hoechst 33342 dye (10 μg/mL; Life Technologies) for 5 min at RT and then visualized under an inverted fluorescence microscope. EdU-free hHF-MSCs served as a negative control.

hHF-MSCs from the 2D and 3D cultures on day 6 were incubated in a fresh medium containing 10 μM of EdU for 24 h at 37 °C in 5 % CO_2 and then harvested by trypsinization, collected as well as centrifuged. The supernatant was removed by aspiration. Cell pellets were washed with 1 mL 1 % bovine serum albumin (BSA; Roche Diagnostics, Mannheim, Germany)/PBS and stained with Apollo® 488 solution for 30 min at RT, according to the manufacturer's instructions. After washing twice with PBS, the cells were analyzed on a FACS Calibur instrument (BD Biosciences, San Jose, CA, USA). The percentage of EdU-labeled cells was evaluated with Cell Quest Pro software (BD Biosciences). EdU-free hHF-MSCs served as a negative control.

Cell cycle assay

Cell cycle assay was performed as described elsewhere (Krishan 1975). hHF-MSCs were collected separately from the 2D and 3D cultures on day 6 and washed twice with ice-cold PBS. After fixing with 70 % ice-cold ethanol (Beijing Huagongchang), hHF-MSCs were incubated at 4 °C for 24 h and washed twice with ice-cold PBS. They were then incubated with RNase A (Beyotime, Shanghai, China) in 0.1 mg/mL PBS at 37 °C for 1 h and then subsequently stained with propidium iodide (Beyotime) in 0.1 mg/mL PBS for 30 min in the dark at RT. The DNA content was determined by flow cytometry and the cell cycle was analyzed.

Colony formation assay

The colony-forming capacity of hHF-MSCs was evaluated. One hundred cells of hHF-MSCs were collected from the 2D and 3D cultures and separately plated in a well of a 6-well plate (in triplicate). The cells were then cultured for
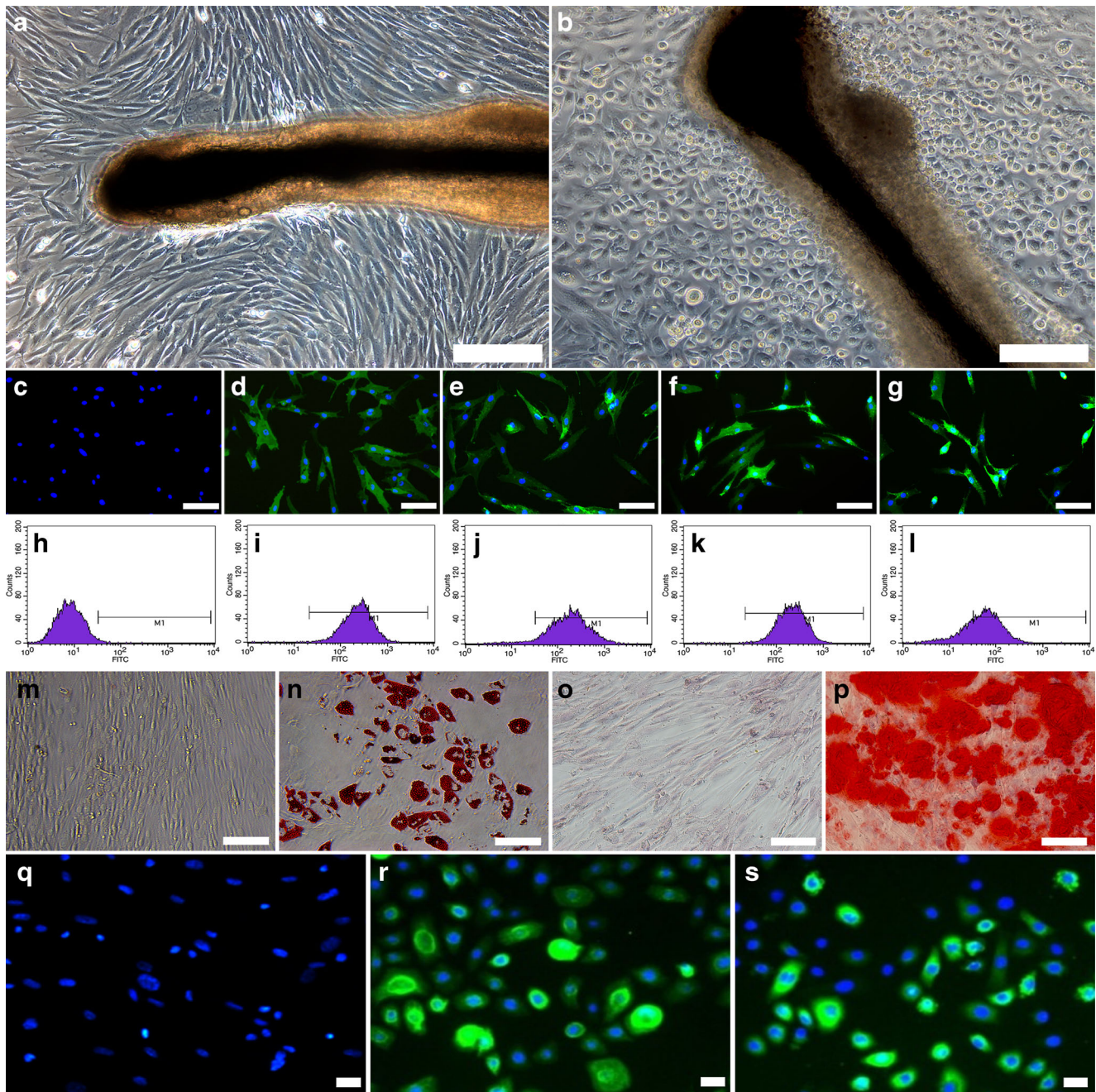
Fig. 1 Organ culture of human hair follicles. Cells migrated out from the hair follicles on day 10 and exhibited a spindle-shaped or cobblestone morphology. The cells that exhibit spindle-shaped morphology were defined as hair follicle-derived mesenchymal stem cells (hHF-MSCs) (**a**). Those that exhibited cobblestone morphology were defined as hair follicle-derived keratinocytes (**b**). *Scale bar* 200 μm. Staining images of cell-surface markers on spindleshaped cells and results of the flow cytometry assay. Spindle-shaped cells expressed CD44, CD73, CD90 and CD105 and stained with secondary antibody served as the negative control. Hoechst 33342 staining was performed to detect nuclear localization (**c**–**g**). *Scale bar* 100 μm. Flow cytometry assays of the spindle-shaped cells show that more than 85 % of the hHF-MSCs in both the 2D and 3D cultures expressed CD44, CD73 and CD90, whereas only 65 % were positive for CD105 (**h**–**l**). The spindle-shaped cells exhibited multipotent differentiation potentials toward adipocytes (**m**, **n**) and osteoblasts (**o**, **p**). *Scale bar* 100 μm. The cobblestone-shaped cells expressed CK14 and CK15. The cobblestone-shaped cells stained with secondary antibody served as the negative control. Hoechst 33342 staining to detect nuclear localization (**q**–**s**). *Scale bar* 20 μm

15 days. At the end of culture, the cells were fixed in 4 % paraformaldehyde and stained with 0.1 % crystal violet

(Sigma-Aldrich) and washed twice with PBS. Colonies were counted under an inverted microscope.

Annexin V staining

Apoptosis was measured by staining the cells with Annexin V using the Apoptosis Kit (Tianjin Sungene Biotech, Tianjin, China) according to the manufacturer's instructions. Briefly, hHF-MSCs from the 2D and 3D cultures on day 6 were collected and washed with buffer, then incubated with Annexin V-FITC and propidium iodide (PI) in the dark at RT for 10 min. At the end of incubation, 500 μL PBS were added to the cells, vortexed gently and subjected to flow cytometry analysis.

Flow cytometry assay and immunofluorescence staining

Flow cytometry and immunofluorescence staining were carried out as described previously (Liu et al. 2010; Mii et al. 2013). After fixing in 4 % paraformaldehyde for 10 min at RT, 1×10^6 hHF-MSCs were washed in PBS and permeabilized in 0.1 % TritonX-100 (RT, 10 min; Sigma-Aldrich). hHF-MSCs were then blocked with 1 % BSA/PBS for 30 min at RT and incubated at 4 °C overnight with mouse anti-human monoclonal antibodies (1:100 dilution, 0.01 % Triton-X-100 in 1 % BSA/PBS): anti-nestin (eBioscience, San Diego, CA, USA), anti-smooth muscle α-actin (α-SMA; Abcam, Cambridge, MA, USA). For surface markers detection, hHF-MSCs were released from the CultiSpher®-G microspheres or tissue culture plates by trypsinization and resuspended in PBS in single cell suspension. After fixing in 4 % paraformaldehyde for 10 min at RT, 1×10^6 cells were washed in PBS and blocked in 1 % BSA /PBS for 30 min at RT. The cells were then incubated at 4 °C overnight with primary mouse anti-human monoclonal antibodies (1:100 dilution): anti-CD90, anti-CD105 (eBioscience), anti-CD44 (R&D Systems, Abingdon, UK) and anti-CD73 (Life Technologies). At the end of incubation, hHF-MSCs were washed twice with PBS and then incubated with Alexa Fluor® 488-conjugated anti-mouse secondary antibody (1 h, RT, 1:400 dilution; Cell Signaling, Danvers, MA, USA). The cells were washed with PBS and then analyzed by flow cytometry. hHF-MSCs that were stained with only the secondary antibody served as a negative control.

hHF-MSCs were seeded on sterile cover slips (Thermo Fisher Scientific, Pittsburg, PA, USA) in 24-well plates at a density of 5×10^5 cells/well and cultured as described above. Then, 24 h after cultivation, hHF-MSCs were fixed with 4 % paraformaldehyde for 15 min at RT, permeabilized in 0.1 % TritonX-100 (RT, 10 min) and blocked with 1 % BSA/PBS for 30 min at RT. Cells were then incubated at 4 °C overnight with mouse anti-human monoclonal antibodies (1:100 dilution, 0.01 % Triton-X-100 in 1 % BSA/PBS): anti-CK14, anti-CK19 (Abcam), anti-nestin, anti-α-SMA. For surface marker detection, hHF-MSCs were fixed

Fig. 2 2D and 3D cultures of hHF-MSCs. hHF-MSCs were seeded onto ▶ gelatin-coated tissue culture plates (2D culture) and on gelatin CultiSpher®-G microbeads (3D culture) at the indicated cell densities and cultured for the indicated times (days). Optically sectioned microbeads from cultures on days 2 and 8 were visualized using acridine orange staining. hHF-MSCs on the surface of the gelatin microbeads gradually increased until all the microbeads were covered by adherent cells in 3D culture groups (**a–n**). *Scale bar* 500 μm. Cell proliferation curves of hHF-MSCs in 3D cultures were plotted using the number of cells counted on each day. hHF-MSCs in the 3D culture proliferated slowly during the first 2 days of cultivation. Starting from day 3, hHF-MSCs in the 3D cultures proliferated quickly, entered the exponential proliferation phase, reaching confluence between day 8 (2000 cells/cm2, 1000 cells/cm2) and day 12 (500 cells/cm2) (**o**). Cell proliferation curves of hHF-MSCs in the 2D cultures were plotted using the number of cells counted on each day (**p**). The average cell proliferation rate was determined by calculating the ratio of increase in cell numbers to the total culture time (**q**). The maximum cell proliferation rate was determined by calculating the ratio of increase in cell numbers to the culture time for the exponential phase (**r**)

with 4 % paraformaldehyde for 15 min at RT and immunofluorescence staining was performed as described above. Nuclear detection was carried out by inverted fluorescence microscopy after DNA staining with Hoechst 33342 dye at 10 μg/mL for 5 min at RT, followed by a rinse in PBS.

Multipotency assay of hHF-MSCs

In order to assess the multi-lineage differentiation potential of the hHF-MSCs on the microcarriers, multipotency assay was performed. The differentiation potentials of hHF-MSCs were evaluated in 24-well plates based on previous studies (Jahoda et al. 2003; Liu et al. 2010). For adipogenic differentiation, the hHF-MSCs from passage 6 were grown in the adipogenic medium consisting of high glucose-Dulbecco's Modified Eagle Medium (HG-DMEM; Life Technologies), 10 % FBS, 1 % P/S, 1 μM dexamethasone (Sigma-Aldrich), 0.5 mM isobutyl-methylxanthine (Sigma-Aldrich), 10 μM insulin (Sigma-Aldrich) and 200 μM indomethacin (Sigma-Aldrich) for 2 weeks. Adipogenic differentiation in the hHF-MSCs was evidenced by the appearance of lipid inclusion vacuoles, which take up the neutral Oil Red O (Sigma-Aldrich). After capturing the images, 200 μL of isopropanol (Beijing Huagongchang) was added to the adipogenic cells in each well of a 24-well plate (in triplicate) and tilted for 20 min at RT to completely dissolve the Oil Red O taken up by the lipid droplet (in' t Anker et al. 2003). The optical density (OD) of Oil Red O extracted from the adipocytes derived from hHF-MSCs was detected at 515 nm using a microplate reader (Infinite M200 PRO; TECAN, Austria).

To determine the maximum absorption wavelength of Oil Red O in isopropanol, Oil Red O was dissolved in isopropanol
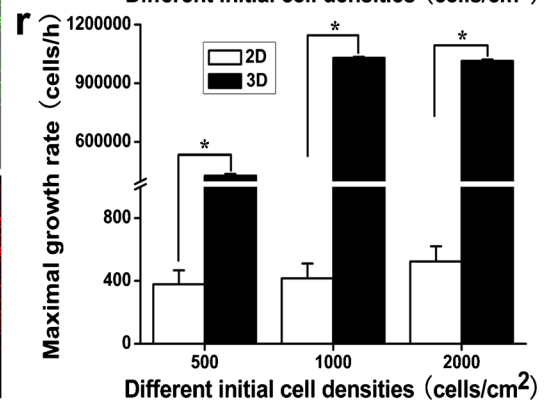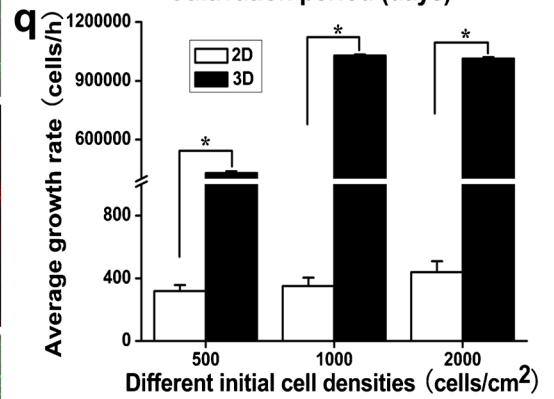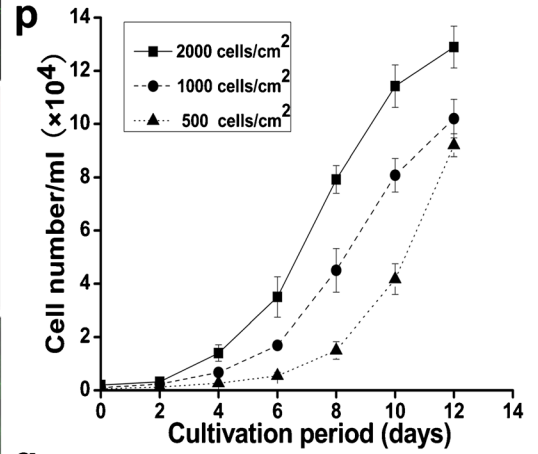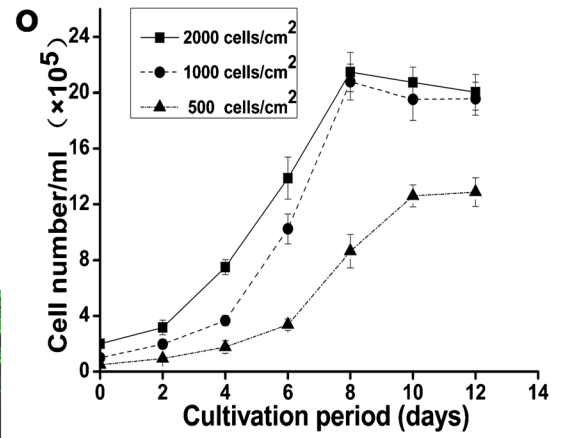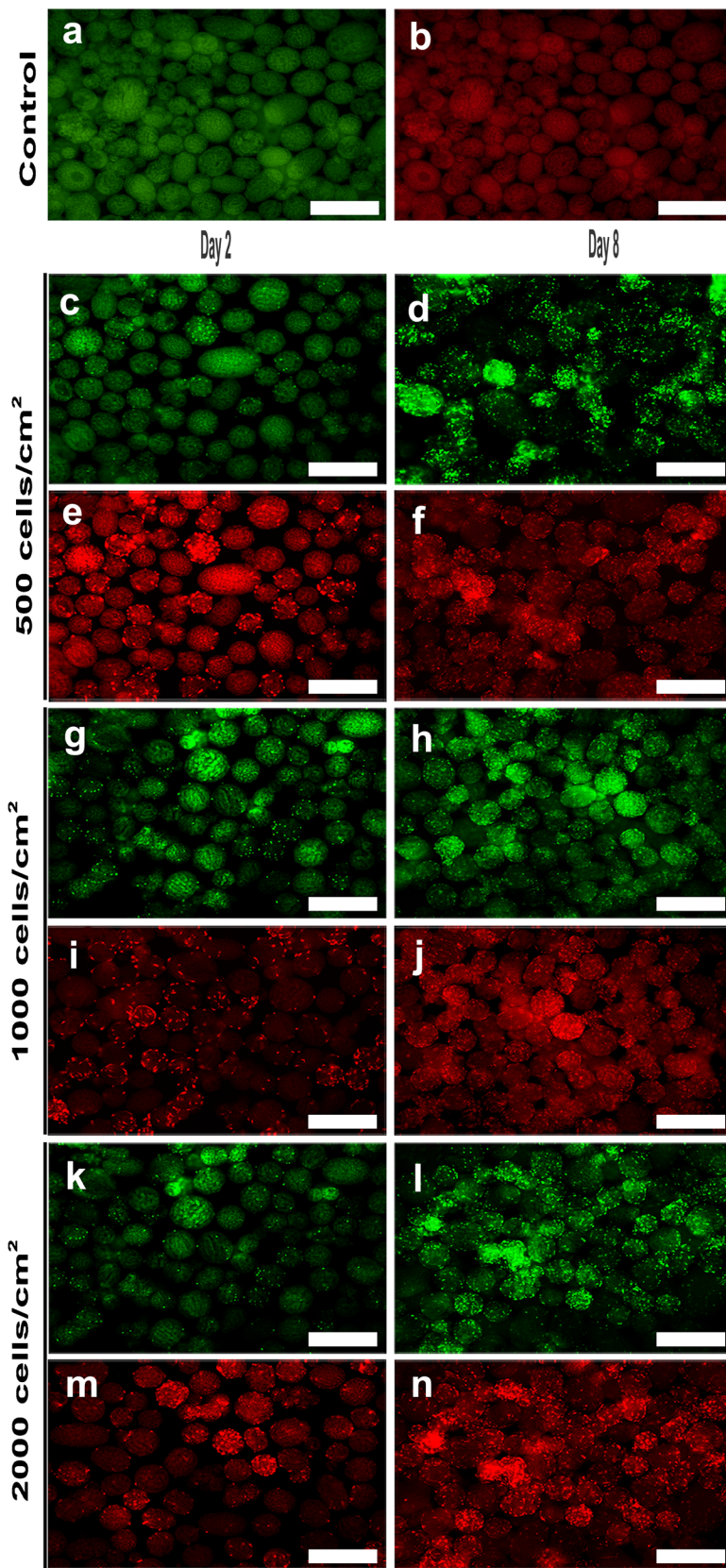
and OD values were measured using a microplate reader at different absorption wavelengths ranging from 465 to 570 nm, with a corresponding increase of 5 nm at each step. After determining the maximum absorption wavelength (515 nm) of Oil Red O in isopropanol, Oil Red O was dissolved in isopropanol to prepare a range of concentrations by serial dilution of the stock solution and subsequently the OD values were read at 515 nm. The standard curve was plotted by using the OD values of Oil Red O at known concentrations, which were further used to calculate the relative concentrations of Oil Red O concentration in adipocytes derived from hHF-MSCs.

For osteogenic differentiation, the hHF-MSCs from passage 6 were cultured in osteogenic medium consisting of HG-DMEM, 10 % FBS, 1 % P/S, 0.1 μM dexamethasone, 50 μM ascorbate-2-phosphate (Sigma-Aldrich) and 10 nM β-glycerophosphate (Sigma-Aldrich). After 4 weeks of culture, Alizarin Red S (Sigma-Aldrich) staining was used to detect the mineralization of calcium salt accumulated in the hHF-MSCs. After being photographed with an inverted microscope, 200 μL of 10 % cetylpyridinium chloride (CPC; Sigma-Aldrich) was added into each well of the 24-well plate (in triplicate) to dissolve the calcium salt–Alizarin Red S complex (in' t Anker et al. 2003). The OD values of the calcium salt–Alizarin Red S complexes were measured using a microplate reader.

To determine the maximum absorption wavelength of the calcium salt–Alizarin Red S complex in 10 % CPC, the calcium salt–Alizarin Red S complex was dissolved in 10 % CPC and OD values were measured using a microplate reader at different absorption wavelengths ranging from 510 to 600 nm, with a corresponding increase of 5 nm at each step. After determining the maximum absorption wavelength at 555 nm, the calcium salt–Alizarin Red S complexes were dissolved in 10 % CPC to prepare a range of concentrations by serial dilution and the OD values of the calcium salt–Alizarin Red S complexes of various serial dilutions were measured. The standard curve was plotted by employing the OD values of the calcium salt–Alizarin Red S complexes at known concentrations, which was used to calculate the relative concentrations of the calcium salt–Alizarin Red S complex in osteocytes derived from hHF-MSCs.

For myogenic induction, hHF-MSCs from passage 6 were cultured in DMEM/F-12 containing 10 % FBS and 5 ng/mL transforming growth factor-beta 1 (TGF-β1; PeproTech) for 7 days. Myogenic differentiation was evaluated as expression of α-SMA by immunofluorescence staining and flow cytometry (Bajpai et al. 2012).

Following the differentiation of the hHF-MSCs into adipocytes, osteoblasts and myocytes, the total RNA was extracted from differentiated cells using Trizol (Life Technologies)

reagent following the manufacturer's instructions. cDNA was synthesized from 1 μg total RNA using EasyScript Reverse Transcriptase (Beijing TransGen Biotech, Beijing, China) in a 50-μL reaction mixture. cDNAs were amplified by PCR to detect the gene expressions of adipocyte lipid-binding protein (aP2), runt-related transcription factor 2 (RunX2) and α-SMA in hHF-MSCs (Bajpai et al. 2012; Jahoda et al. 2003; Liu et al. 2010). The relative expression level of glyceraldehyde-3-phsosphate dehydrogenase (GAPDH) was used as an internal control to normalize the specific gene expression in each sample.

Real-time PCR (qPCR) was performed with 2 μL of the cDNA sample with SYBR Green PCR Master Mix (Roche Diagnostics) using the ABI Prism 7300 Sequence Detection System (Applied Biosystems, Foster City, CA, USA). The fold change in cDNAs of the target gene and the control was determined by using the following formula: fold change $2^{-\Delta\Delta Ct}$, where $\Delta\Delta Ct = (Ct_{Target} - Ct_{GAPDH})_{sample} - (Ct_{Target} - Ct_{GAPDH})_{control}$ (Livak and Schmittgen 2001). The primer sequences used were: GAPDH: forward primer 5′-ACATCA AGAAGGTGGTGAAGCAGG-3′, reverse primer 5′-CAGC GTCAAAGGTGGAGGAGTGG-3′, product length 123 bp (NCBI Reference Sequence: XM_005253678.1). RunX2: forward primer 5′-TGGTTAATCTCCGCAGGTCAC-3′, reverse primer 5′-ACTGTGCTGAAGAGGCTGTTTG-3′, product length 143 bp (NCBI Reference Sequence: NM_001015051.3). aP2: forward primer 5′-AAAGAAGT AGGAGTGGGCTTTGC-3′, reverse primer 5′-CCCCATTC ACACTGATGATCAT-3′, product length 79 bp (NCBI Reference Sequence: NM_001442.2), α-SMA: forward primer 5′-CTGTTCCAGCCATCCTTCAT-3′, reverse primer 5′-TCATGATGCTGTTGTAGGTGGT-3′, product length 70 bp (NCBI Reference Sequence: NM_001613.2). All the primers were designed by NCBI/Primers-BLAST and synthesized by Sangon Biotech, China.

Statistical analyses

Data are expressed as mean±standard deviation. Multiple comparisons were analyzed using analysis of variance (ANOVA) or Student's t test followed by Bonferroni correction. $P<0.05$ was considered statistically significant.

Results

### Derivation of MSCs from human hair follicles

As previously reported (Liu et al. 2010; Wang et al. 2013; Zhang et al. 2013), cells that displayed either spindle-shaped (Fig. 1a) or cobblestone morphology (Fig. 1b) migrated out from hair follicles between days 7 and 10 and proliferated in the tissue culture plates. The cells with spindle-shaped

Fig. 3 EdU incorporation assay. hHF-MSCs in the 2D and 3D cultures were detected using EdU. EdU-positive cells and representative images of fields show *green-colored* proliferation cells. Hoechst 33342 staining was performed to detect nuclear localization (**a**–**f**). *Scale bar* 20 μm. Flow cytometry assay to detect the proliferation of hHF-MSCs by EdU incorporation (**g**–**l**). Percentage of EdU was plotted as the mean±SD of triplicate samples from 3 independent experiments (**m**)
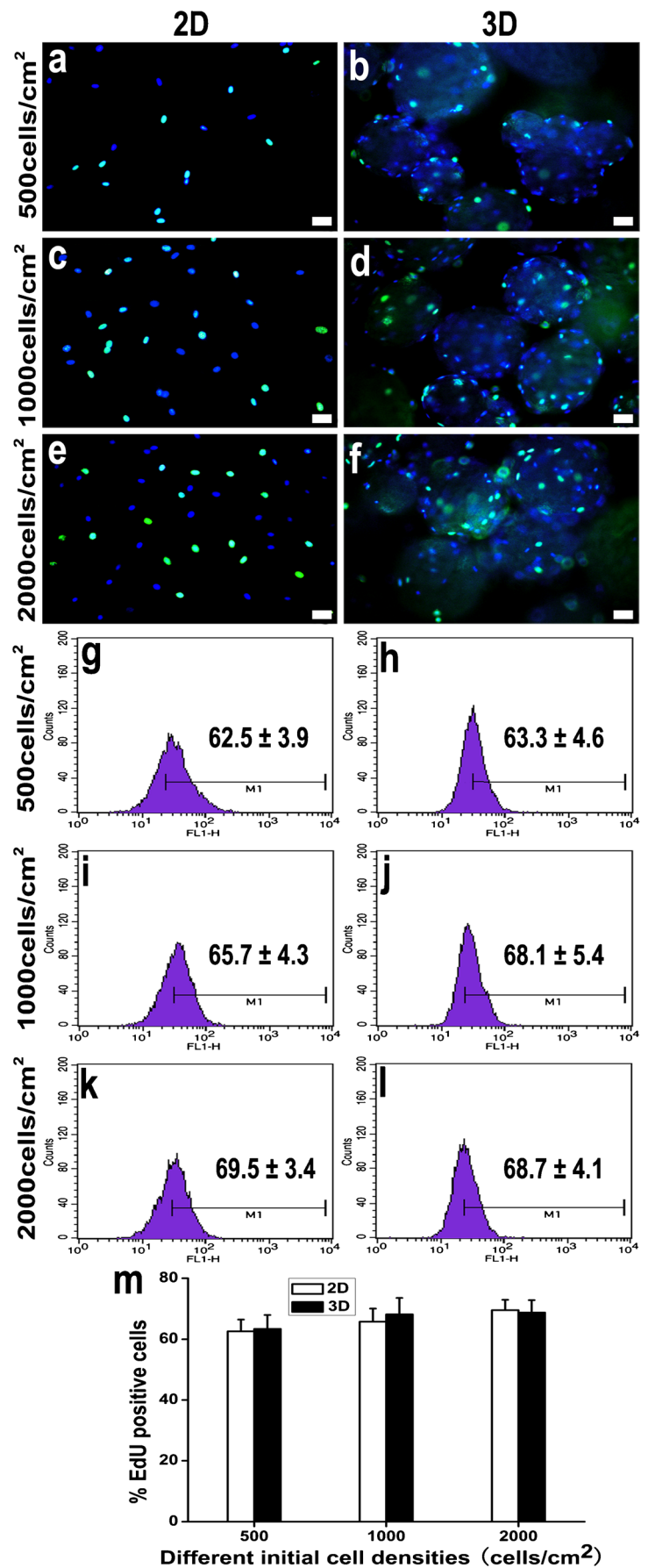
Fig. 4 Cell cycle assay. Propidium iodide staining and flow cytometry analysis were performed to detect the cell cycles of hHF-MSCs in 2D and 3D cultures (**a–f**). The percentage of hHF-MSCs (with different initial cell densities from the 2D and 3D cultures) in the G1, S and G2 phases of the cell cycle was comparatively analyzed (**g–i**). All values were plotted as the mean±SD of triplicate samples from 3 independent experiments
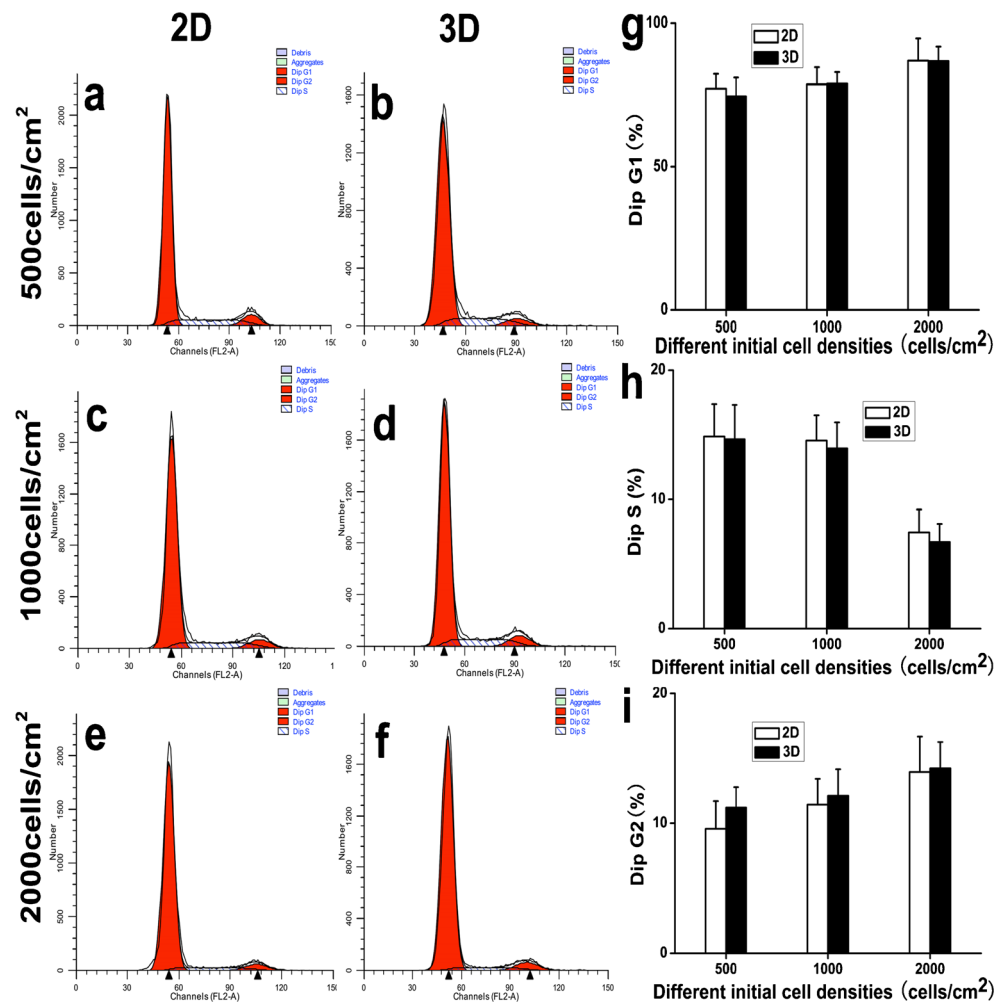
morphology were collected, pooled and subjected to phenotypic characterization and multipotency assay. The spindle-shaped cells that expressed the MSC differentiation markers, CD44, CD73, CD90 and CD105 (Fig. 1c-i) and possessed multipotent differentiation potentials towards adipocytes (Fig. 1m, n) and osteoblasts (Fig. 1o, p) were defined as hHF-MSCs. Cells with a cobblestone morphology were collected, pooled and phenotypically characterized and found to express the keratinocyte markers CK14 and CK19 (Fig. 1q-s, Kruger et al. 1999).

Proliferation of hHF-MSCs in 2D and 3D culture

Acridine orange labeling showed that hHF-MSCs adhered to the CultiSpher®-G microbeads emitted red and green fluorescence and increased in number during culture (Fig. 2a–n).The hHF-MSCs in the 3D culture contained in the gelatin microbeads quickly entered the exponential proliferation phase by day 2 post-culture and reached a plateau on day 8 (2000 cells/cm², 1000
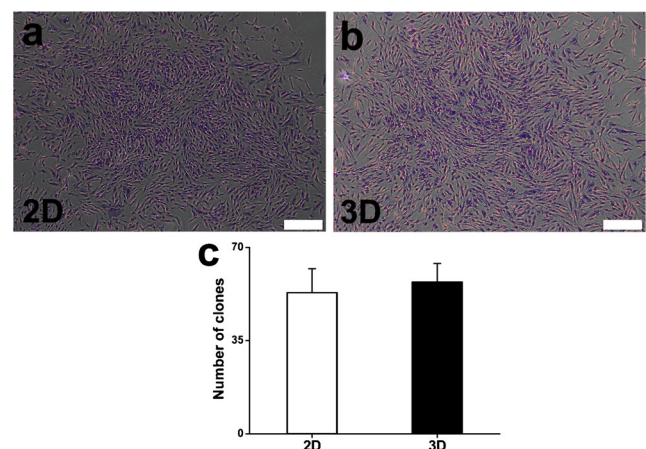
Fig. 5 Colony formation assay. The colony-forming capacity of hHF-MSCs in the 2D and 3D cultures was evaluated. Individual colonies stained with crystal violet and captured at ×4 magnification for the 2D and 3D cultures (**a, b**). *Scale bar* 200 μm. Colonies were counted under an inverted microscope (**c**). Average number of colonies generated per 100 cells by cells in the 2D and 3D cultures plotted as the mean±SD of triplicate samples from 3 independent experiments

cells/cm^2) (Fig. 2o). Notably, the spinner culture with a cell density of 500 cells/cm^2 also exhibited a high proliferation potential on day 8 and reached a plateau on day 10 (Fig. 2o). In contrast, the hHF-MSCs in the 2D culture proliferated slowly during the first 2 days of cultivation (Fig. 2p). From day 3 onwards, the proliferation of hHF-MSCs increased rapidly, wherein they entered the exponential proliferation phase and reached confluence between day 8 (2000 cells/cm^2) and day 10 (1000 cells/cm^2, 500 cells/cm^2), whilst displaying a high proliferation potential on day 10 (Fig. 2p). The hHF-MSCs seeded at various densities quickly adhered to and proliferated well on the microspheres, thus generating at least hundreds of millions of hHF-MSCs on 1 g of CultiSpher®-G within 12 days, resulting in a cumulative cell expansion of greater than 26-fold. The average and the maximum cell proliferation rates of hHF-MSCs seeded at different cell densities in the 3D culture were significantly higher when compared to those in the 2D culture (Fig. 2q, r).

In agreement with the cell proliferation curves, the hHF-MSCs in the 2D and 3D cultures displayed an active EdU incorporation on day 6. Flow cytometry revealed that more than 60 % of the hHF-MSCs in both the 2D and 3D cultures displayed active EdU uptake (Fig. 3a–m). Consistent with the cell proliferation assays and acridine orange labeling, the cell cycle assay analysis demonstrated a significantly high number

of hHF-MSCs in the G1 phase in the 3D and 2D cultures (about 80 %; Fig. 4a–i). On the contrary, only a few cells progressed to the S and G2 phase in the 3D and 2D cultures (about 10 %; Fig. 4a–i). Colony formation assays were performed on the 3D and 2D cultured hHF-MSCs, which showed no significant difference (Fig. 5a–c). Annexin V staining showed the 3D and 2D cultures contained fewer apoptotic cells in comparison to cultures expanded under standard conditions, although the difference did not reach significance (Fig. 6a–h).

Cell-surface marker profiling of hHF-MSCs in 2D and 3D culture

Cell-surface marker profiles have been considered to be one of the principal determinants of MSCs differentiation (Minguell et al. 2001). As expected, immunofluorescence analysis showed that the hHF-MSCs from both the 2D and 3D cultures expressed CD44, CD73, CD90, CD105 and nestin (Fig. 7a–l). However, a positive expression of flow cytometry analysis further revealed that more than 80 % of the hHF-MSCs in both the 2D and 3D culture expressed CD44, CD73, CD90 and nestin, while only 65 % were found to be positive for CD105 (Fig. 7m–x). Cell-surface marker profiles and fluorescence intensity were similar in both the 2D and 3D cultures (Fig. 7y, z).

Fig. 6 Cell apoptosis assay. hHF-MSC from the 2D and 3D cultures on day 6 were incubated with Annexin V and PI and analyzed by flow cytometry (**a**–**f**). The percentage of Annexin V- and PI-positive hHF-MSCs in the 2D and 3D cultures was comparatively analyzed (**g**, **h**). All the percentages were plotted as the mean±SD of triplicate samples from 3 independent experiments
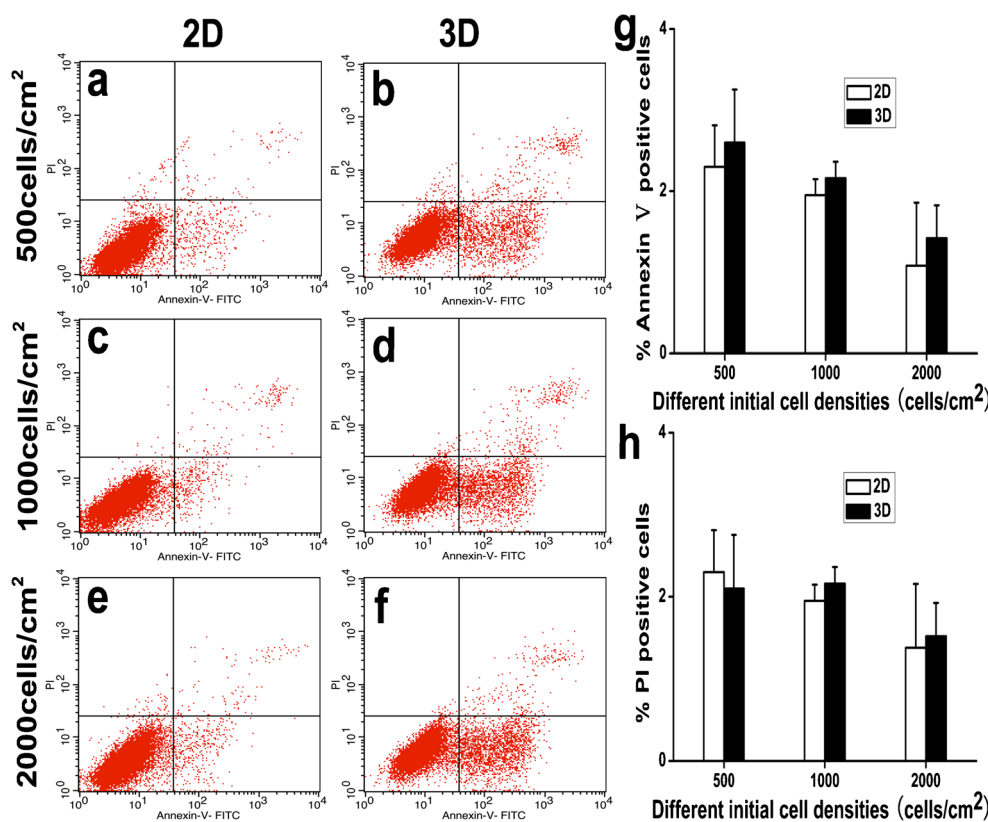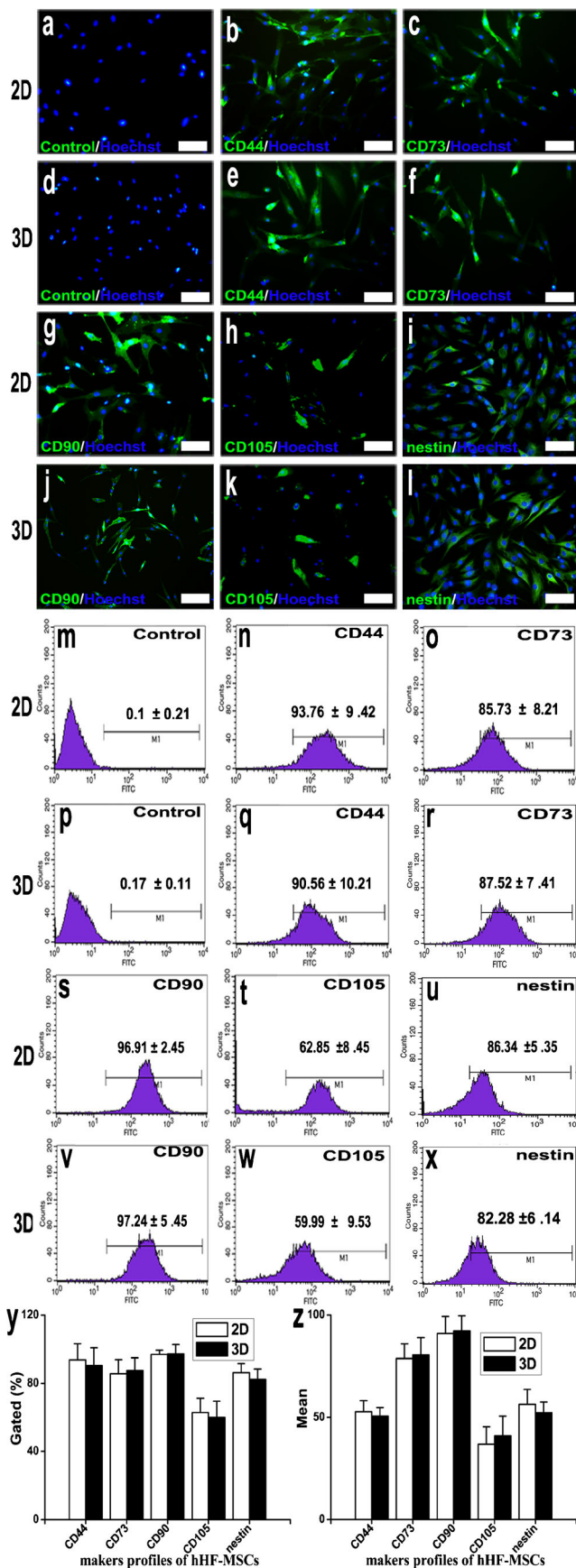
◀ **Fig. 7** Staining of cell-surface markers on hHF-MSCs and flow cytometry assay. hHF-MSCs in 2D and 3D cultures were immunostained with cell-surface markers and subjected to flow cytometry assay. The hHF-MSCs expressed CD44, CD73, CD90 and CD105 (**a**–**l**). hHF-MSCs stained with secondary antibody served as the negative control. Hoechst 33342 staining was performed to detect nuclear localization. Representative images are shown from one of the 3 independent experiments. *Scale bar* 100 μm. Flow cytometry assay results showing the expression of hHF-MSCs markers in the 2D or 3D cultures (**m**–**x**). Gated data were plotted as the mean±SD of triplicate samples from 3 independent experiments (**y**). Average fluorescence intensity was plotted as the mean±SD of triplicate samples from 3 independent experiments (**z**)

Multipotent differentiation potential of hHF-MSCs in 2D and 3D cultures

In addition, we examined the effect of prolonged in vitro expansion on the differentiation potential of hHF-MSCs. To this end, hHF-MSCs were differentiated towards the osteogenic, adipogenic, or myogenic lineages in passage 6. The degree of differentiation was assessed by lineage-specific functional assays, namely Oil Red O stain for adipogenesis, Alizarin S stain for osteogenesis and flow cytometry analysis for α-SMA expression. Adipogenesis was confirmed by the presence of lipid droplets in the cytoplasm of the hHF-MSCs derived from both the 2D and 3D cultures, as evidenced by Oil Red O staining (Fig. 8a–h). To quantify adipogenesis of hHF-MSCs under adipogenic culture conditions, the maximum absorption wavelength of Oil Red O was determined at 515 nm (Fig. 8i) and a standard curve was plotted (Fig. 8j). Biochemical quantification analysis showed there were no statistically significant differences in the lipid accumulation (Fig. 8k) between the hHF-MSCs derived from the two cultures. In agreement with the findings of the biochemical analysis, the results of the RT-PCR indicated that, under adipogenic culture conditions, the hHF-MSCs from both the cultures expressed the adipogenic gene, *aP2* (Fig. 8l). Further, qPCR analysis confirmed that there was no significant difference in the expression level of *aP2* (Fig. 8m) between the hHF-MSCs derived from both the cultures.

Alizarin S staining showed that, under osteogenic culture conditions, calcium nodules were deposited on the surface of the hHF-MSCs derived from both cultures (Fig. 9a–h). To quantify osteogenesis of the hHF-MSCs under osteogenic culture conditions, the maximum absorption wavelength of the calcium salt–Alizarin Red S complex was determined at 555 nm (Fig. 9i) and a standard curve was plotted (Fig. 9j). Biochemical quantification demonstrated that under osteogenic culture conditions there were no statistically significant differences in calcium deposition (Fig. 9k) between the hHF-MSCs derived

from the two cultures. These data were in agreement with the results of the PCR assay. RT-PCR analysis demonstrated that, under osteogenic culture conditions, the hHF-MSCs from both the cultures expressed the osteogenic gene, *RunX2* (Fig. 9l). However, there was no significant difference in the expression level of *RunX2* (Fig. 9m) between the hHF-MSCs from the two cultures.

As expected, immunofluorescence analysis showed that, under myogenic culture conditions, the hHF-MSCs from both the 2D and 3D cultures expressed α-SMA (Fig. 10a-c). However, flow cytometry further revealed that more than 60 % of the hHF-MSCs in both cultures expressed α-SMA and α-SMA profiles were similar in the 2D and 3D cultures (Fig. 10d). These data were in agreement with the results of the PCR assay. RT-PCR analysis demonstrated that, under myogenic culture conditions, hHF-MSCs from both cultures expressed the myogenic gene α-SMA (Fig. 10e). However, no significant difference in the expression level of α-SMA (Fig. 10f) was noted between the hHF-MSCs from the two cultures.

Discussion

Mesenchymal stem cells represent a potentially powerful tool in regenerative medicine, owing to their multi-lineage differentiation potentials, wide variety of sources and remarkable efficacies in tissue repair and regeneration. Ideally, the success of any MSCs therapy relies upon the presence of large quantities of autologous stem cells that possess a high proliferation capacity and exhibit the potential for full differentiation (Hodgkinson et al. 2009; Sun et al. 2011).

In the present study, we employed the CultiSpher®-G microbeads as microcarriers for the 3D culture of hHF-MSCs and spinning bottles as bioreactors to generate hHF-MSCs on a large scale. It is noteworthy that the hHF-MSCs displayed high proliferation potential over several passages (n=3). As many as hundreds of millions of hHF-MSCs were generated on 1 g of CultiSpher®-G in the 3D culture within 12 days, wherein there was a 26-fold increase in the cell number, significantly higher than hBM-MSCs and human placenta derived MSCs (Chen
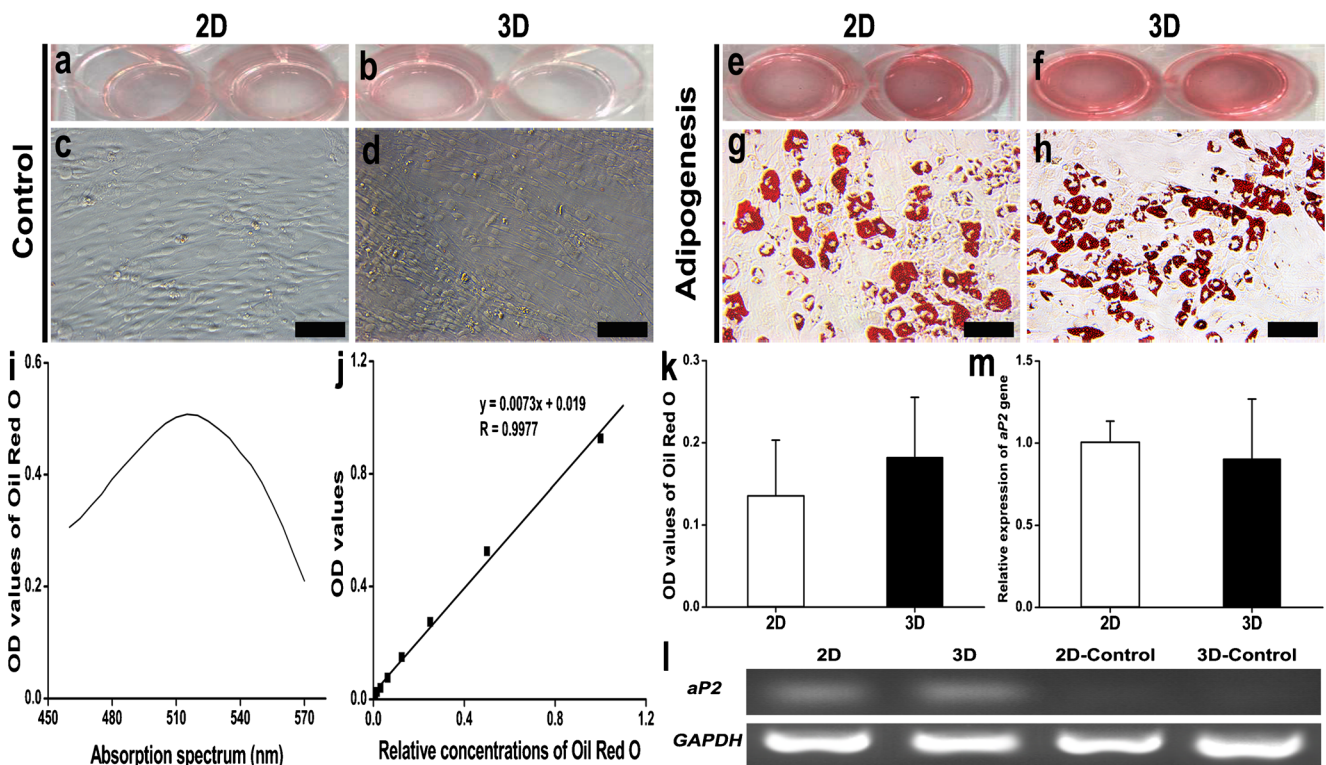
Fig. 8 Adipogenic differentiation assay. hHF-MSCs derived from the 2D and 3D cultures were cultured in adipogenic differentiation medium for 2 weeks. Lipid droplets accumulating in the hHF-MSCs during adipogenesis were stained red with Oil Red O (**a**–**h**) and quantified by a biochemical assay (**k**). Representative images are shown from one of the 3 independent experiments. *Scale bar* 100 μm. The maximum absorption wavelength of Oil Red O in isopropanol was determined at 515 nm (**i**). The standard curve was created by plotting OD values against relative concentrations of Oil Red O (*R*=0.9977) (**j**). Total RNA was extracted from the hHF-MSCs during adipogenesis, reverse-transcribed to cDNA and quantified by qPCR to determine the expression levels of the adipogenic marker aP2 in hHF-MSCs. Reverse transcription and PCR (**l**) and qPCR (**m**) showed no statistically significant differences in gene expression levels during adipogenesis between hHF-MSCs in the 2D and 3D cultures
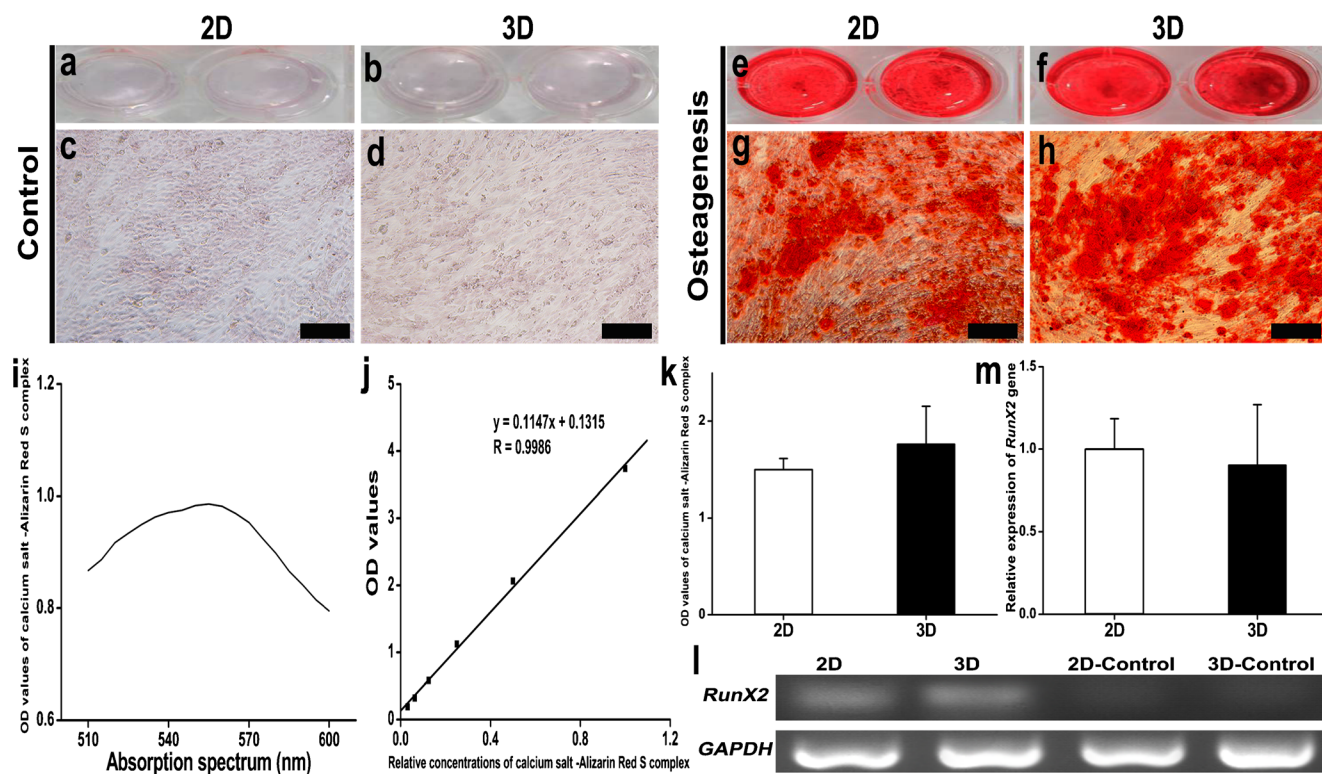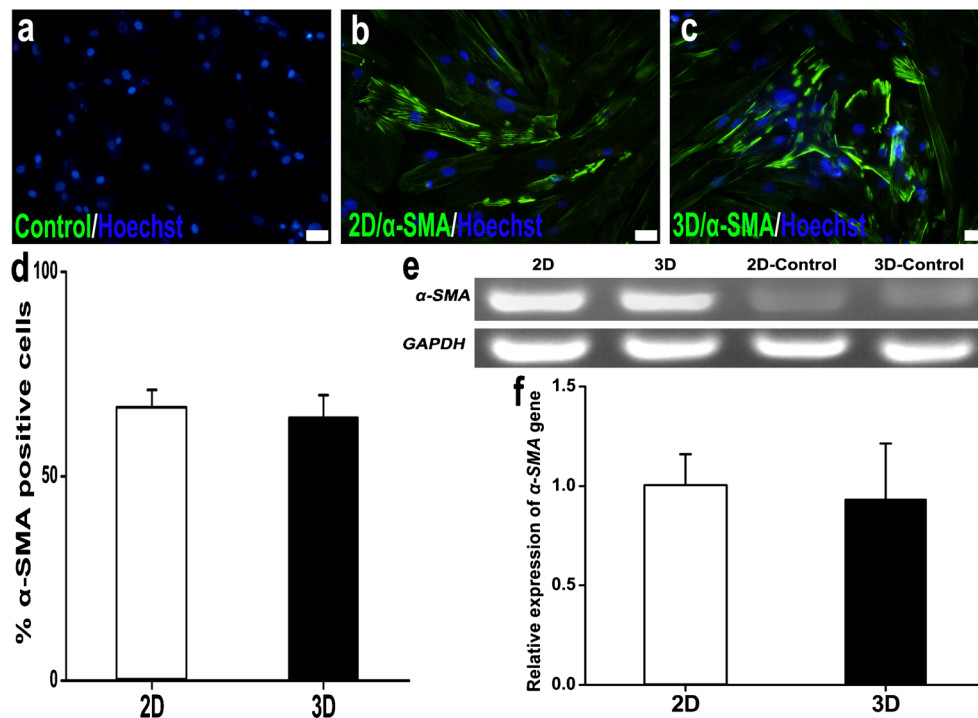
Fig. 9 Osteogenic differentiation assay. The hHF-MSCs derived from the 2D and 3D cultures were cultured in osteogenic differentiation medium for 4 weeks. Calcium salt accumulated in the hHF-MSCs under osteogenic differentiation conditions and stained red with Alizarin Red S (**a**–**h**) and quantified by a biochemical assay (**k**). Representative images are shown from one of 3 independent experiments. *Scale bar* 100 μm. The maximum absorption wavelength of the calcium salt–Alizarin Red S in 10 % cetylpyridinium chloride was determined at 555 nm (**i**). The standard curve was created by plotting OD values against relative concentrations of calcium salt–Alizarin Red S ($R=$ 0.9986) (**j**). Total RNA was extracted from the hHF-MSCs during osteogenesis, reverse-transcribed to cDNA and quantified by qPCR to determine the expression levels of the osteogenic marker RunX2. Reverse transcription and PCR (**l**) and qPCR (**m**) showed no statistically significant differences in the gene expression levels during osteogenesis between hHF-MSCs in the 2D and 3D cultures

et al. 2011; Sun et al. 2010). Based on the average number of population doublings per passage (2.5–3.5), it was estimated that hHF-MSCs underwent approximately ~36 population doublings during the first 12 passages. The addition of the 8–10 population doublings that took place during the initial isolation and expansion phase resulted in ~45 population doublings (Bajpai et al. 2012). This compares favorably with previous reports estimating 13–25 population doublings for hBM-MSCs (Wagner et al. 2008), although a more accurate comparison would require that both hHF-MSCs and hBM-MSCs be isolated from the same donors and account for sex and age differences. Regardless, during the first 2 weeks of cell isolation, a single scalp hair follicle could give rise to approximately 5×10^4 MSCs, which then undergo ~36 additional population doublings yielding ~10^{15} cells (Bajpai et al. 2012). Given that the density of hair follicles in the scalp is over 200 follicles/cm^2 (Barman et al. 1965) and that most of them are in the anagen phase for prolonged times, the potential of hHF-MSC as a stem cell source for regenerative medicine is very promising. Further, the robust expansion of hHF-MSCs precludes the potential risks of tumorigenesis due to mutations caused by repeated subculturing.

Conventional 2D cultures of stem cells suffer from several limitations such as inherent variability between culture vessels, lack of control of many culture parameters, low cell production yields, high cost, labor intensiveness, technical handling issues and an inability to expand within a short time for further transplantation of stem cells, thus rendering them unsuitable for clinical and industrial purposes (Chen et al. 2013; Martin et al. 2011; Yuan et al. 2012). Moreover, replicative cell senescence and terminal differentiation potential associated with repeated subculturing for scaled-up generation of MSCs, hinder its feasibility in cell therapy. It is therefore imperative to employ the 3D cell culture approach for large-scale production of MSCs, in particular with the use of microcarriers in bioreactors. Accumulating data on 3D stem cell culture suggest that they are reproducible, scalable and cost-effective, maintain stem cell potency as well as facilitate stem cell expansion and, therefore, demonstrate high feasibility in clinical practice (Chen et al. 2013; Martin et al. 2011;

Fig. 10 Myogenic differentiation assay. The hHF-MSCs derived from the 2D and 3D cultures were cultured in myogenic differentiation medium for 1 week. Immunofluorescence analysis showed that the hHF-MSCs from both the 2D and 3D cultures expressed α-SMA (**a–c**). hHF-MSCs stained with secondary antibody served as the negative control. Hoechst 33342 staining was performed to detect nuclear localization. Representative images are shown from one of 3 independent experiments. *Scale bar* 20 μm. Flow cytometry assay of hHF-MSCs in both the 2D and 3D cultures expressed α-SMA. Percentage of α-SMA positive cells was plotted as the mean±SD of triplicate samples from 3 independent experiments (**d**). Total RNA was extracted from the hHF-MSCs during myogenesis, reverse-transcribed to cDNA and quantified by qPCR to determine the expression levels of the myogenic marker, α-SMA. Reverse transcription and PCR (**e**) and qPCR (**f**) showed no statistically significant differences in the gene expression levels during myogenesis between the hHF-MSCs in the 2D and 3D cultures

Yuan et al. 2012). The use of microbeads as microcarriers for 3D cell culture has displayed promising results over 2D culture in obtaining MSCs on a large scale (Choi et al. 2011; Liu et al. 2004b; Schop et al. 2010; Timmins et al. 2012; Yuan et al. 2012). The macroporous, CultiSpher microcarriers have a high surface area to volume ratio, thus providing larger cell culture surfaces within a defined culture space.

Several previous studies have demonstrated CultiSpher to yield the highest seeding efficiency and growth, achieving a higher fold expansion and a greater final cell density (Rubin et al. 2007; Timmins et al. 2012; Wu et al. 2003). Several reports have demonstrated the use of the gelatin-based biodegradable CultiSpher microcarriers for direct transplantation (Chen et al. 2011, 2013; Liu et al. 2004b; Yang et al. 2007; Zhou et al. 2011). Yang et al. employed these microcarriers for in vivo transplantation, wherein the rat BM-MSCs entrapped in the microspheres were implanted into bone defects (Yang et al. 2007). Another study by Chen et al. used these microcarriers for in vitro generation of centimeter-sized bone tissue (Chen et al. 2011). Zhou et al. used experimentally produced biodegradable MCs like gelatin beads and fabricated micronized dermal matrix and small intestinal sub mucosa for direct implantation into mice (Zhou et al. 2011). Owing to the

biodegradability and a good biocompatibility of this microcarrier matrix in the body, the gelatin microbeads could not only be used as microcarriers for 3D culture but also as cell delivery vehicles in direct transplantation. By using gelatin microbeads as carriers for cell culture, earlier studies amplified hBM-MSCs or human adipose-derived MSCs, which retained their cell surface markers and multipotency (Kim et al. 2009; Rubin et al. 2007). Direct administration of autologous keratinocytes or melanocytes cultured on macroporous gelatin microbeads have successfully resurfaced diabetic leg ulcers or re-pigmented vitiligo (Liu et al. 2004a, b).

The main component of CultiSpher®-G microbeads is gelatin. The gelatin coating affects engagement of cell adhesion molecules (e.g., integrins), which influence proliferation activity and cell survival. Thus, 2D culture on gelatin-coated culture dishes was used as a control to exclude the possibility that the gelatin influences proliferation. To visualize the localization of hHF-MSCs on the CultiSpher®-G microspheres, acridine orange staining was performed. Acridine orange is a sensitive fluorescent dye that fluoresces green when bound to dsDNA and red when bound to ssDNA or RNA. The green and red fluorescence images are presented individually

(Fig. 2a–n). The hHF-MSCs were found to be distributed on the surface of the gelatin microbeads and exhibited high cell numbers. Next, we performed a cell proliferation assay with "click" chemistry to detect the progression of S-phase in hHF-MSCs.

In 3D culture, hHF-MSC expansion began with a 1-day lag phase prior to exponential growth, although lag phase growth rates did not differ in cultures seeded at different densities. In contrast, the length of the lag phase was inversely proportional to initial seeding density in 2D culture. This phenomenon resulted in supernal average and maximum growth rates for hHF-MSCs expanded in 3D culture versus those in 2D culture. In our experiment, EdU was incorporated by hHF-MSCs derived from 2D and 3D cultures at day 6, indicating active DNA synthesis consistent with the cell proliferation curves in exponential phase. Meanwhile, Annexin V staining showed that hHF-MSCs in 3D culture hardly undergo apoptosis as cells in the 2D culture do.

The hHF-MSCs derived from 3D and 2D cultures expressed MSCs markers CD44, CD73, CD90 and CD105, as well as nestin (Fig. 7m–x). Previous studies have shown that nestin-expressing hair follicle stem cells differentiate into neurons (Amoh et al. 2005c; Duong et al. 2012; Hoffman 2006, 2007; Mii et al. 2013). Thus, the hHF-MSCs derived from 3D culture possess great therapeutic potential.

Multipotency is a hallmark of MSCs differentiation (Jahoda et al. 2003; Liu et al. 2010; Minguell et al. 2001). Self-renewal and multipotent differentiation potential, which are determined by intrinsic cell regulatory elements and the external environment, are the main characteristics of MSCs (Jaenisch and Bird 2003; Ji et al. 2011; Minguell et al. 2001). The success of stem cell therapy depends not only upon the quantities of cells harvested but also on the multipotency of MSCs. Therefore, the maintenance of multipotent MSCs is of great interest (Martin et al. 2011; Sun et al. 2011). bFGF is a well-known growth factor in the maintenance of the self-renewing and multipotent differentiation capacities of the MSCs (Ito et al. 2007; Li and Zhao 2014; Liu et al. 2010; Zhang et al. 2013). As a consequence, bFGF was used as a routine supplement in our culture medium system to maintain the self-renewal and multipotency of the hHF-MSCs. Indeed, above 80 % of hHF-MSCs cultured on the CultiSpher®-G in 3D culture remained in G0/G1 phase, indicating that they were quiescent (Minguell et al. 2001). Furthermore, the hHF-MSCs in the 3D culture retained their potential to differentiate towards adipocytes, osteoblasts and myoblasts as did those in the 2D culture. Moreover, the biochemical quantification, flow cytometry analysis and qPCR assays revealed that there were no significant differences between the adipogenic, osteogenic and myoblasts differentiation of the hHF-MSCs from the 2D and 3D cultures.

To the best of our knowledge, the present study is the first of its kind to quantify adipogenesis and osteogenesis of hHF-MSCs by biochemical analysis. Until now, the assessment of the differentiation of MSCs to mesoderm lineages has only been demonstrated by immunohistochemical analysis without a quantitative assessment of the differentiation efficiency to a specific lineage (Chen et al. 2013; in' t Anker et al. 2003). To accurately assess adipogenesis and osteogenesis of the hHF-MSCs derived from 2D and 3D cultures, we quantified the concentrations of Oil Red O or calcium salt–Alizarin Red S complexes accumulated in the hHF-MSCs. Interestingly, the findings of the biochemical analysis were corroborated by those of the qPCR assay, wherein there were no statistically significant differences in the levels of the gene expressions of the adipogenic gene, *aP2* and the osteogenic gene, *RunX2*, in the hHF-MSCs derived from the 2D and 3D cultures.

In conclusion, we demonstrated the robust in vitro long-term expansion of hHF-MSCs by using CultiSpher®-G microcarriers. Further, our study proved the feasibility of hHF-MSC/CultiSpher®-G microcarrier constructs in 3D culture for their potential applicability in regenerative medicine.

References

Amoh Y, Li L, Campillo R, Kawahara K, Katsuoka K, Penman S, Hoffman RM (2005a) Implanted hair follicle stem cells form Schwann cells that support repair of severed peripheral nerves. Proc Natl Acad Sci U S A 102:17734–17738

Amoh Y, Li L, Hamada Y, Katsuoka K, Hoffman RM (2005b) Multipotent nestin-positive, keratin-negative hair-follicle bulge stem cells can form neurons. J Investig Dermatol 125:A5

Amoh Y, Li L, Katsuoka K, Penman S, Hoffman RM (2005c) Multipotent nestin-positive, keratin-negative hair-follicle bulge stem cells can form neurons. Proc Natl Acad Sci U S A 102:5530–5534

Amoh Y, Li L, Katsuoka K, Hoffman RM (2008) Multipotent hair follicle stem cells promote repair of spinal cord injury and recovery of walking function. Cell Cycle 7:1865–1869

Bajpai VK, Mistriotis P, Andreadis ST (2012) Clonal multipotency and effect of long-term in vitro expansion on differentiation potential of human hair follicle derived mesenchymal stem cells. Stem Cell Res 8:74–84

Barman JM, Astore I, Pecoraro V (1965) The Normal Trichogram of the Adult. J Invest Dermatol 44:233–236

Chen M, Wang X, Ye Z, Zhang Y, Zhou Y, Tan WS (2011) A modular approach to the engineering of a centimeter-sized bone tissue construct with human amniotic mesenchymal stem cells-laden microcarriers. Biomaterials 32:7532–7542

Chen AK, Reuveny S, Oh SK (2013) Application of human mesenchymal and pluripotent stem cell microcarrier cultures in cellular

therapy: achievements and future direction. Biotechnol Adv 31: 1032–1046

Choi JS, Kim BS, Kim JD, Choi YC, Lee EK, Park K, Lee HY, Cho YW (2011) In vitro expansion of human adipose-derived stem cells in a spinner culture system using human extracellular matrix powders. Cell Tissue Res 345:415–423

Duong J, Mii S, Uchugonova A, Liu F, Moossa AR, Hoffman RM (2012) Real-time confocal imaging of trafficking of nestin-expressing multipotent stem cells in mouse whiskers in long-term 3-D histoculture. In Vitro Cell Dev Biol Anim 48:301–305

Hayashi M, Sofuni T, Ishidate M Jr (1983) An application of Acridine Orange fluorescent staining to the micronucleus test. Mutat Res 120: 241–247

Higgins CA, Itoh M, Inoue K, Richardson GD, Jahoda CAB, Christiano AM (2012) Reprogramming of Human Hair Follicle Dermal Papilla Cells into Induced Pluripotent Stem Cells. J Investig Dermatol 132: 1725–1727

Hodgkinson T, Yuan XF, Bayat A (2009) Adult stem cells in tissue engineering. Expert Rev Med Devices 6:621–640

Hoffman RM (2006) The hair follicle and its stem cells as drug delivery targets. Expert Opin Drug Deliv 3:437–443

Hoffman RM (2007) The potential of nestin-expressing hair follicle stem cells in regenerative medicine. Expert Opin Biol Ther 7:289–291

in't Anker PS, Noort WA, Scherjon SA, Kleijburg-van der Keur C, Kruisselbrink AB, van Bezooijen RL, Beekhuizen W, Willemze R, Kanhai HH, Fibbe WE (2003) Mesenchymal stem cells in human second-trimester bone marrow, liver, lung, and spleen exhibit a similar immunophenotype but a heterogeneous multilineage differentiation potential. Haematologica 88:845–852

Ito T, Sawada R, Fujiwara Y, Seyama Y, Tsuchiya T (2007) FGF-2 suppresses cellular senescence of human mesenchymal stem cells by down-regulation of TGF-beta2. Biochem Biophys Res Commun 359:108–114

Jaenisch R, Bird A (2003) Epigenetic regulation of gene expression: how the genome integrates intrinsic and environmental signals. Nat Genet 33:245–254

Jahoda CAB, Whitehouse CJ, Reynolds AJ, Hole N (2003) Hair follicle dermal cells differentiate into adipogenic and osteogenic lineages. Exp Dermatol 12:849–859

Ji SZ, Xiao SC, Luo PF, Huang GF, Wang GY, Zhu SH, Wu MJ, Xia ZF (2011) An epidermal stem cells niche microenvironment created by engineered human amniotic membrane. Biomaterials 32:7801–7811

Kim I, Park H, Shin Y, Kim M (2009) Adipogenic Differentiation of Adipose-Derived Stem Cells on Collagen Microbeads. Tissue Eng Regen Med 6:924–930

Krishan A (1975) Rapid flow cytofluorometric analysis of mammalian cell cycle by propidium iodide staining. J Cell Biol 66:188–193

Kruger K, Blume-Peytavi U, Orfanos CE (1999) Basal cell carcinoma possibly originates from the outer root sheath and or the bulge region of the vellus hair follicle. Arch Dermatol Res 291:253–259

Lako M, Armstrong L, Cairns PM, Harris S, Hole N, Jahoda CA (2002) Hair follicle dermal cells repopulate the mouse haematopoietic system. J Cell Sci 115:3967–3974

Li Y, Zhao X (2014) Concise review: Fragile X proteins in stem cell maintenance and differentiation. Stem Cells 32:1724–1733

Li L, Mignone J, Yang M, Matic M, Penman S, Enikolopov G, Hoffman RM (2003) Nestin expression in hair follicle sheath progenitor cells. Proc Natl Acad Sci U S A 100:9958–9961

Liu JY, Hafner J, Dragieva G, Burg G (2004a) Bioreactor microcarrier cell culture system (Bio-MCCS) for large-scale production of autologous melanocytes. Cell Transplant 13:809–816

Liu JY, Hafner J, Dragieva G, Seifert B, Burg G (2004b) Autologous cultured keratinocytes on porcine gelatin microbeads effectively heal chronic venous leg ulcers. Wound Repair Regen 12:148–156

Liu JY, Peng HF, Andreadis ST (2008) Contractile smooth muscle cells derived from hair-follicle stem cells. Cardiovasc Res 79:24–33

Liu JY, Peng HF, Gopinath S, Tian J, Andreadis ST (2010) Derivation of functional smooth muscle cells from multipotent human hair follicle mesenchymal stem cells. Tissue Eng Part A 16:2553–2564

Liu F, Uchugonova A, Kimura H, Zhang C, Zhao M, Zhang L, Koenig K, Duong J, Aki R, Saito N, Mii S, Amoh Y, Katsuoka K, Hoffman RM (2011) The bulge area is the major hair follicle source of nestin-expressing pluripotent stem cells which can repair the spinal cord compared to the dermal papilla. Cell Cycle 10:830–839

Livak KJ, Schmittgen TD (2001) Analysis of relative gene expression data using real-time quantitative PCR and the 2(T)(-Delta Delta C) method. Methods 25:402–408

Lutz SE, Lengfeld J, Agalliu D (2014) Stem cell-based therapies for multiple sclerosis: recent advances in animal models and human clinical trials. Regen Med 9:129–132

Martin Y, Eldardiri M, Lawrence-Watt DJ, Sharpe JR (2011) Microcarriers and their potential in tissue regeneration. Tissue Eng B 17:71–80

Mii S, Uehara F, Yano S, Tran B, Miwa S, Hiroshima Y, Amoh Y, Katsuoka K, Hoffman RM (2013) Nestin-Expressing Stem Cells Promote Nerve Growth in Long-Term 3-Dimensional Gelfoam(R)-Supported Histoculture. PLoS ONE 8:e67153

Minguell JJ, Erices A, Conget P (2001) Mesenchymal stem cells. Exp Biol Med (Maywood) 226:507–520

Motaln H, Schichor C, Lah TT (2010) Human mesenchymal stem cells and their use in cell-based therapies. Cancer 116:2519–2530

Olmer R, Haase A, Merkert S, Cui W, Palecek J, Ran C, Kirschning A, Scheper T, Glage S, Miller K, Curnow EC, Hayes ES, Martin U (2010) Long term expansion of undifferentiated human iPS and ES cells in suspension culture using a defined medium. Stem Cell Res 5:51–64

Peng HF, Liu JY, Andreadis ST, Swartz DD (2011) Hair follicle-derived smooth muscle cells and small intestinal submucosa for engineering mechanically robust and vasoreactive vascular media. Tissue Eng Part A 17:981–990

Phillips HJ, Terryberry JE (1957) Counting actively metabolizing tissue cultured cells. Exp Cell Res 13:341–347

Pittenger MF, Mackay AM, Beck SC, Jaiswal RK, Douglas R, Mosca JD, Moorman MA, Simonetti DW, Craig S, Marshak DR (1999) Multilineage potential of adult human mesenchymal stem cells. Science 284:143–147

Rubin JP, Bennett JM, Doctor JS, Tebbets BM, Marra KG (2007) Collagenous microbeads as a scaffold for tissue engineering with adipose-derived stem cells. Plast Reconstr Surg 120:414–424

Salic A, Mitchison TJ (2008) A chemical method for fast and sensitive detection of DNA synthesis in vivo. Proc Natl Acad Sci U S A 105: 2415–2420

Sart S, Schneider YJ, Agathos SN (2009) Ear mesenchymal stem cells: An efficient adult multipotent cell population fit for rapid and scalable expansion. J Biotechnol 139:291–299

Sart S, Agathos SN, Li Y (2013) Engineering stem cell fate with biochemical and biomechanical properties of microcarriers. Biotechnol Prog 29:1354–1366

Schop D, van Dijkhuizen-Radersma R, Borgart E, Janssen FW, Rozemuller H, Prins HJ, de Bruijn JD (2010) Expansion of human mesenchymal stromal cells on microcarriers: growth and metabolism. J Tissue Eng Regen Med 4:131–140

Shim KJ, Han I (2007) Use of hair follicular cells for cultured skin substitutes. Tissue Eng Regen Med 4:191–196

Sun LY, Hsieh DK, Yu TC, Chiu HT, Lu SF, Luo GH, Kuo TK, Lee OK, Chiou TW (2009) Effect of pulsed electromagnetic field on the proliferation and differentiation potential of human bone marrow mesenchymal stem cells. Bioelectromagnetics 30:251–260

Sun LY, Hsieh DK, Syu WS, Li YS, Chiu HT, Chiou TW (2010) Cell proliferation of human bone marrow mesenchymal stem cells on biodegradable microcarriers enhances in vitro differentiation potential. Cell Prolif 43:445–456

Sun LY, Lin SZ, Li YS, Harn HJ, Chiou TW (2011) Functional cells cultured on microcarriers for use in regenerative medicine research. Cell Transplant 20:49–62

Timmins NE, Kiel M, Gunther M, Heazlewood C, Doran MR, Brooke G, Atkinson K (2012) Closed system isolation and scalable expansion of human placental mesenchymal stem cells. Biotechnol Bioeng 109:1817–1826

Uchugonova A, Duong J, Zhang N, Konig K, Hoffman RM (2011) The bulge area is the origin of nestin-expressing pluripotent stem cells of the hair follicle. J Cell Biochem 112:2046–2050

Wagner W, Horn P, Castoldi M, Diehlmann A, Bork S, Saffrich R, Benes V, Blake J, Pfister S, Eckstein V, Ho AD (2008) Replicative senescence of mesenchymal stem cells: a continuous and organized process. PLoS ONE 3:e2213

Wang YM, Liu JY, Tan XH, Li GF, Gao YH, Liu XJ, Zhang LH, Li YL (2013) Induced pluripotent stem cells from human hair follicle mesenchymal stem cells. Stem Cell Rev Rep 9:451–460

Wu QF, Wu CT, Dong B, Wang LS (2003) Cultivation of human mesenchymal stem cells on macroporous CultiSpher G microcarriers. Zhongguo Shi Yan Xue Ye Xue Za Zhi 11:15–21

Wu C, Liu F, Li P, Zhao G, Lan S, Jiang W, Meng X, Tian L, Li G, Li Y, Liu JY (2014) Engineered hair follicle mesenchymal stem cells overexpressing controlled-release insulin reverse hyperglycemia in mice with type 1 diabetes. Cell Transplant. doi:10.3727/096368914X681919

Yang Y, Rossi FM, Putnins EE (2007) Ex vivo expansion of rat bone marrow mesenchymal stromal cells on microcarrier beads in spin culture. Biomaterials 28:3110–3120

Yuan Y, Kallos MS, Hunter C, Sen A (2012) Improved expansion of human bone marrow-derived mesenchymal stem cells in microcarrier-based suspension culture. J Tissue Eng Regen Med 8(3):210–225

Zhang X, Wang Y, Gao Y, Liu X, Bai T, Li M, Li L, Chi G, Xu H, Liu F, Liu JY, Li Y (2013) Maintenance of high proliferation and multipotent potential of human hair follicle-derived mesenchymal stem cells by growth factors. Int J Mol Med 31:913–921

Zhou Y, Yan Z, Zhang H, Lu W, Liu S, Huang X, Luo H, Jin Y (2011) Expansion and delivery of adipose-derived mesenchymal stem cells on three microcarriers for soft tissue regeneration. Tissue Eng Part A 17:2981–2997